Nanoscale

Accepted Manuscript

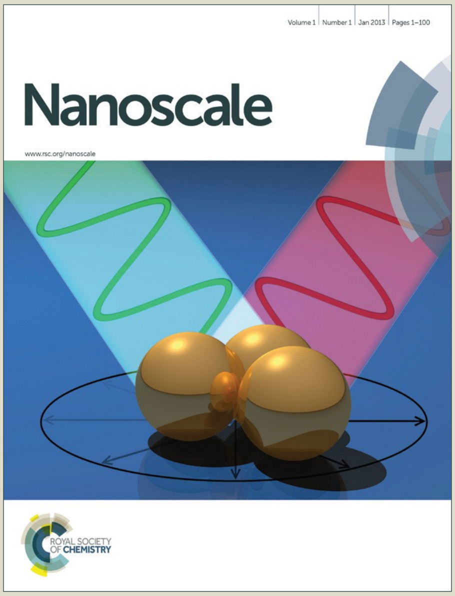

ROYAL SOCIETY OF CHEMISTRY

www.rsc.org/nanoscale

Solution synthesis of telluride-based nano-barbell structures coated with PEDOT:PSS for spray-printed thermoelectric generators

Eun Jin Bae, Young Hun Kang, Kwang-Suk Jang, Changjin Lee, and Song Yun Cho*

Division of Advanced Materials, Korea Research Institute of Chemical Technology, 141 Gajeong-ro, Yuseong-gu, Daejeon 34114, Republic of Korea

Electronic supplementary information (ESI) available: Synthetic procedure of Te–Bi_2Te_3/PEDOT:PSS hybrids, fabrication of thermoelectric generators by spray-printing, measurements of thermoelectric properties, and solution images, XRD patterns, TEM-EDAX, and SEM-EDAX of Te–Bi_2Te_3/PEDOT:PSS hybrids.

Telluride-based heterostructures coated with solution-processable poly(3,4-ethylenedioxythiophene):poly(styrenesulfonate) (Te–Bi_2Te_3/PEDOT:PSS) were synthesized through a solution-phase reaction at low temperature. The water-based synthesis yielded PEDOT:PSS-coated Te–Bi_2Te_3 nano-barbell structures with a high Seebeck coefficient that can be stably dispersed in water. These hybrid solutions were deposited onto a substrate by the spray-printing method to prepare thermoelectric generators. The thermoelectric properties of the Te–Bi_2Te_3/PEDOT:PSS hybrid films were significantly enhanced by a simple acid treatment due to the increased electrical conductivity, and the power factor of those materials can be effectively tuned over a wide range depending on the acid concentration of the treatment. The power factors of the synthesized Te–Bi_2Te_3/PEDOT:PSS hybrids were optimized to 60.05 $\mu W\ m^{-1}\ K^{-2}$ with a Seebeck coefficient of 93.63 $\mu V\ K^{-1}$ and electrical conductivity of 69.99 $S\ cm^{-1}$. The flexible thermoelectric generator fabricated by spray-printing Te–Bi_2Te_3/PEDOT:PSS hybrid solutions showed an open-circuit voltage of 1.54 mV with six legs at $\Delta T = 10$ °C. This approach presents the potential for realizing printing-processable hybrid thermoelectric materials for application in flexible thermoelectric generators.

Thermoelectric energy conversion is an attractive and environmentally friendly way to recover energy from industrial waste heat or natural heat because of its potential for improving the energy efficiency. The thermoelectric generator (TEG) is an interesting heat engine that can convert a temperature difference directly into electrical voltage via the Seebeck effect. The Seebeck coefficient is an essential indicator of thermoelectric conversion efficiency and the most widely measured property specific to thermoelectric materials. The performance of thermoelectric materials can be expressed as a dimensionless thermoelectric figure of merit $ZT = S^2\sigma T/\kappa$, where S is the Seebeck coefficient, σ is the electrical conductivity, κ is the thermal conductivity, and T is the absolute temperature.[1,2] The figure of merit of thermoelectric materials can be significantly improved by constructing one-dimensional or two-dimensional nanostructures owing to the enhanced phonon scattering at nanoscale interfaces and grain boundaries.[3-5] Especially, nanowire heterostructures can take advantage of phonon scattering at the nanowire surface and compositional interfaces, which can provide a much higher power factor.[6-9] Many ongoing studies have reported that low-dimensional nanostructured thermoelectric materials based on Te or Bi_2Te_3 can improve the thermoelectric performance.[10-12] However, the insufficient electrical conductivity of most Te-based nanostructures (approximately 3 S cm^{-1}) reduces their thermoelectric performance and prevents their wide application.[13]

The synthetic methods of various nanostructures have mainly been based on the chemical vapor deposition process. Hot press methods have been predominantly used to fabricate thermoelectric devices using nanostructured powder. Therefore, obtaining high-quality thermoelectric nanostructures with a high thermoelectric performance in a simple manner is still a great challenge. In addition, developing easy and simple methods to fabricate thermoelectric devices by using nanostructured materials, which can be suitable for low-cost and flexible thermoelectric devices, is still a problem. This is because the hot press method is unavoidable without solution-processable thermoelectric nanostructures, which can be stably dispersed in a solution. To introduce nanostructured thermoelectric materials into the solution process, these materials should possess stable dispersity in a solution and good inherent thermoelectric properties without a "hot" process.

Here, we show a simple synthesis of Te–Bi_2Te_3 nanowire heterostructures with a narrow diameter and length distribution that are coated with poly(3,4-ethylenedioxythiophene):poly(styrenesulfonate) (PEDOT:PSS) in order to produce a TEG by the simple spray-printing process. In the suggested method, PEDOT:PSS is used as a conducting polymer in order to disperse Te–Bi_2Te_3 nanowire heterostructures uniformly into water. The PEDOT:PSS that surrounds the Te–Bi_2Te_3 nanowire heterostructures can also play a significant role in enhancing the electrical conductivity. We also demonstrate the effect of acid treatment on the thermoelectric properties of soluble Te–Bi_2Te_3/PEDOT:PSS hybrids. Our study proved that the thermoelectric performance of Te–Bi_2Te_3/PEDOT:PSS hybrids can be enhanced by tuning the improved electrical conductivity with acid treatment. Furthermore, flexible TEGs were fabricated by the spray-printing method that were composed of only p-type Te–Bi_2Te_3/PEDOT:PSS patterns. To the best of our knowledge, spray-printed organic thermoelectric films and TEGs have not yet been reported. We believe that this suggested convenient synthesis of soluble Te–Bi_2Te_3/PEDOT:PSS hybrids and spray-printed TEGs can potentially be applied to flexible thermoelectric power generators.

The synthesis of water-soluble Te–Bi_2Te_3/PEDOT:PSS hybrids was carried out with sodium telluride and bismuth chloride in the presence of ascorbic acid and PEDOT:PSS at 60 °C. The formation of Te–Bi_2Te_3 nanowire heterostructures was first characterized by using X-ray diffraction (XRD) (Fig. S1). The spectra clearly indicated the partial formation of Bi_2Te_3 with Te. The shape of the nanowire heterostructures of Te–Bi_2Te_3 with PEDOT:PSS was further confirmed with a transmission electron microscope (TEM), as shown in Fig. 1. The TEM images clearly demonstrated Te–Bi_2Te_3 nanowire heterostructures (nano-barbell structures) that were coated with a PEDOT:PSS thin layer. On the surface of a nano-barbell, PEDOT:PSS can assist with the uniform dispersion of Te–Bi_2Te_3 nanowire heterostructures in water. Te–Bi_2Te_3 nanowires without PEDOT:PSS encapsulation showed no stable water dispersion (Fig. S2), which can clog the nozzle during the spray or inkjet printing process. The nano-barbell was measured to have a diameter of 30–40 nm and length of 300–500 nm for the nanobar and diameter of 50–60 nm for the nanoplate. A TEM-energy dispersive spectrometer (TEM-EDAX) was used to analyze the composition of the Te–Bi_2Te_3/PEDOT:PSS hybrids, as shown in Fig. S3. While Te was detected in both the nanobar and nanoplate parts of the nano-barbell structure, the majority of Bi was observed in the nanoplate area. The TEM-EDAX analysis confirmed Te–Bi_2Te_3 nanowire heterostructures with a barbell shape containing Te in the nanobar and Bi_2Te_3 in the nanoplates.

The Te–Bi_2Te_3/PEDOT:PSS hybrid solutions were simply deposited by the spray-printing method to fabricate thin thermoelectric films (Fig. S4). H_2SO_4 treatment was then used to enhance the thermoelectric properties of the Te–Bi_2Te_3/PEDOT:PSS films. To investigate the thermoelectric properties of Bi_2Te_3-PEDOT:PSS hybrid films treated with various concentrations of H_2SO_4, the electrical conductivity, Seebeck coefficient, and power factor ($S^2\sigma$) of those thin films were measured at room temperature. Fig. 2a shows the electrical conductivity and Seebeck coefficient of the Te–Bi_2Te_3/PEDOT:PSS hybrid films. The electrical conductivity significantly increased from 8.21 to 87.01 S cm^{-1} as the H_2SO_4 concentration of the treatment was increased, whereas the Seebeck coefficient decreased from 141.02 to 80.11 μV K^{-1}. Fig. 2b shows the power factor of the Te–Bi_2Te_3/PEDOT:PSS hybrids after treatment with various concentrations of H_2SO_4. The average power factor of the non-treated Te–Bi_2Te_3/PEDOT:PSS was 16.33 μW m^{-1} K^{-2}, while the optimized average power factor of the 80% H_2SO_4-treated film was 60.05 μW m^{-1} K^{-2}. The power factor of H_2SO_4-treated Te–Bi_2Te_3/PEDOT:PSS hybrid films was much higher than that of non-treated films because of the notable enhancement of the electrical conductivity by the H_2SO_4 treatment. We believe that the increased electrical conductivity of the Te–Bi_2Te_3/PEDOT:PSS hybrids was mainly due to the nanostructural rearrangement of PEDOT:PSS, which was interconnected on the surface of the Te–Bi_2Te_3 nano-barbell structures, and the removal of PSS by the acid treatment.[14,15]

Fig. 3 shows scanning electron microscope (SEM) images of the surface morphologies of Te–Bi_2Te_3/PEDOT:PSS hybrids depending on the H_2SO_4 concentration of the treatment. The Te–Bi_2Te_3/PEDOT:PSS hybrid films before H_2SO_4 treatment consisted of nano-barbell structures that were densely packed together and interconnected with each other. The surface of the nano-barbell structures was also smooth and clear. The structures were stably maintained and interconnected even after 100 vol% H_2SO_4 treatment without any chopping phenomena. Interestingly, however, the plate parts of the nano-barbells were slightly damaged by the treatment with highly concentrated H_2SO_4, as shown in Fig. 3. The size of the *plate* in the nano-barbell was diminished, and the edge parts of the plate become stubby, especially with 100 vol% H_2SO_4. To confirm the compositional change of Te–Bi_2Te_3/PEDOT:PSS hybrids by H_2SO_4 treatment, the hybrid films were analyzed by SEM-EDAX mapping, as shown in Fig. S5 and Table S1. The atomic percentages for Bi and Te in Te–Bi_2Te_3/PEDOT:PSS hybrid films without H_2SO_4 treatment were found to be 20.17% and 79.83%, respectively. Although the stoichiometric ratio between Bi and Te in Bi_2Te_3 is 2:3, that of Te–Bi_2Te_3/PEDOT:PSS hybrids is approximately 1:4 because the nanobar part in the nano-barbell structure mainly consists of Te with negligible amounts of Bi. The ratio of Bi gradually decreased from 20.17% to 2.95% as the H_2SO_4 concentration was increased, whereas the ratio of Te increased from 79.83% to 97.05%. This means that the amount of Bi decreased relative to Te in Te–Bi_2Te_3/PEDOT:PSS hybrids due to the partial removal of the nanoplates, which mainly contain Bi_2Te_3, by the acid treatment. Even though the Seebeck coefficient of our Te–Bi_2Te_3/PEDOT:PSS hybrids was lower than those of previously reported Te (408 μV K^{-1} at 298 K) or Bi_2Te_3 (155 μV K^{-1} at 298 K) due to the absence of a high-temperature process,[16,17] the power factor can be optimized by the significantly enhanced electrical conductivity of PEDOT:PSS with H_2SO_4 treatment. Such high electrical conductivity compensated for the lower Seebeck coefficient of our hybrids due to the lack of a high-temperature press. Thus, our hybrids provide a higher power factor than those of previously reported thermoelectric nanostructures (2.7–8.6 μW m^{-1} K^{-2} with an electrical conductivity of 0.08–3.59 S cm^{-1}).[16,17]

To confirm the ability of H_2SO_4 treatment to induce conformational and compositional changes in Te–Bi_2Te_3/PEDOT:PSS hybrid films, the surface chemical compositions of the films were analyzed by X-ray photoelectron spectroscopy (XPS). Fig. 4 shows Bi 4f and Te 3d peaks of the Te–Bi_2Te_3/PEDOT:PSS hybrid films treated with H_2SO_4 of various concentrations. The peaks at 157.3 and 162.8 eV correspond to the reported values for the binding energies of Bi $4f_{7/2}$ and Bi $4f_{5/2}$, respectively, of Bi_2Te_3. The peaks at about 158.9 and 164.4 eV in the Bi 4f region also existed for the higher binding energy of Bi_2Te_3. Additionally, the peaks at 572.5 and 583 eV correspond to the reported values for the binding energies of Te $3d_{5/2}$ and Te $3d_{3/2}$, respectively, of Bi_2Te_3. In the Te 3d region, the peaks at about 158.9 and 164.4 eV were also observed for the higher binding energy of Bi_2Te_3.[17,18] Those peaks in the higher binding energy were caused by the oxidized states of Bi and Te atoms from the oxidized surface. This oxidized state occurred because the surface of the Te–Bi_2Te_3 nanostructured films was rapidly covered with a mixed Bi_2O_3 and TeO_2 layer by O_2 adsorption during the synthesis.[19] In our study, the Te–Bi_2Te_3/PEDOT:PSS hybrids were synthesized in water under ambient atmosphere, and the Te–Bi_2Te_3 nano-barbell structures surrounded by PEDOT:PSS were finally dispersed in water. Therefore, the surface of the solution-based Te–Bi_2Te_3 can possess more oxidized states of Bi and Te than that of Te or Bi_2Te_3 nanostructures synthesized via solid-based methods. For these reasons, the peaks of the Bi_2Te_3 binding energy were weaker than those of the oxidation binding energy. However, the characteristic peaks of Bi-O and Te-O states were clearly reduced after acid treatment. In most cases, the oxidation layer is critical to thermoelectric properties. The prevention of oxidation of Bi_2Te_3 nanostructures has been reported to be especially significant to enhancing the thermoelectric properties of Bi_2Te_3 nanocomposites.[20] Even though water-based synthesis generates more oxidized states, simply using acid can significantly reduce the oxidation layer. Interestingly, Fig. 4a shows that the oxidized state in Bi 4f decreased more profoundly than that in Te 3d as the concentration of the H_2SO_4 treatment was increased. This suggests that the oxidized form of Bi can be more effectively removed by H_2SO_4 treatment than that of Te because Bi is mainly located in the nanoplate area, where it is easily damaged by H_2SO_4 as shown in the SEM surface images.

The TEGs of Te–Bi_2Te_3/PEDOT:PSS hybrids were fabricated on a glass or flexible polyimide. To fabricate the TEGs, Te–Bi_2Te_3/PEDOT:PSS patterns were spray-printed by using a showdown mask (Fig. 5a). Because spray-printing is one of the easiest methods to form a pattern of active materials, it is suitable for large-area devices. Fig. 5b shows a TEG composed of 15 legs arranged on the glass substrate with the printed silver electrodes. The flexible TEG was fabricated on the polyimide substrate with the same fabrication method as shown in Fig. 5c. The difference in the electrical potential was derived from the temperature gradient on both sides of the thermoelectric array, which was created by contacting one of the sides with a heat source. To evaluate the total thermoelectric output voltage of the integrated thermoelectric legs, the open circuit voltage (V_{oc}) versus temperature difference (ΔT) based on the number of thermoelectric legs was measured, as shown in Figs. 5d and e. As the number of thermoelectric legs was increased from 1 to 6, the output voltage of the flexible spray-printed TEG gradually increased from 0.31 to 1.54 mV (at ΔT = 10 °C). However, the device performance still needs to be improved by using p–n juctioned device structure and optimizing the design of the device shape.

In summary, Te–Bi_2Te_3 nano-barbell structures incorporating PEDOT:PSS were successfully synthesized in a soluble nanostructured form. Therefore, TEGs can easily be fabricated by a simple spray-printing process without difficult and complicated processing conditions. The thermoelectric properties of the Te–Bi_2Te_3/PEDOT:PSS hybrids were satisfactorily enhanced by tuning the electrical conductivity and Seebeck coefficient by acid treatment. The power factor of the H_2SO_4-treated Te–Bi_2Te_3/PEDOT:PSS hybrids was comparable to or higher than that of hot-pressed Te or Bi_2Te_3 nanostructured materials. This solution-based approach to Te–Bi_2Te_3/PEDOT:PSS hybrids may offer a simple way for fabricating flexible TEGs by using a spray method.

Acknowledgements

This work was supported by a grant from the KRICT Core Project (KK 1507-C06) and the R&D Convergence Program of National Research Council of Science and Technology of the Republic of Korea.

Notes and references

1 J. -F. Li, W. -S. Liu, L. -D. Zhao and M. Zhou, *NPG Asia Mater.,* 2010, **2**, 152.

2 G. J. Snyder and E. S. Toberer, *Nat. Mater.,* 2008, **7**, 105.

3 M. S. Dresselhaus, G. Dresselhaus, X. Sun, Z. Zhang, S. B. Cronin and T. Koga, *Phys. Solid State,* 1999, **41**, 679.

4 T. Sun, X. B. Zhao, T. J. Zhu and J. P. Tu, *Mat. Lett.,* 2006, **60**, 2534.

5 A. I. Hochbaum, R. Chen, R. D. Delgado, W. Liang, E. C. Garnett, M. Najarian, A. Majumdar and P. Yang, *Nature,* 2008, **451**, 163.

6 H. Fang and Y. Wu, *J. Mater. Chem. A,* 2014, **2**, 6004.

7 C. Dames and G. Chen, *J. Appl. Phys.,* 2004*,* **95**, 682.

8 Y. Lin and M. S. Dresselhaus, *Phys. Rev. B,* 2003, **68**, 5304.

9 L. D. Hicks and M. S. Dresselhaus, *Phys. Rev. B,* 1993, **47**, 16631.

10 C. Zhou, C. Jin, X. Li and L. Shi, *Appl. Phys. Lett.,* 2005, **87**, 133109.

11 S. Song, J. Fu, X. Li, W. Gao and H. Zhang, *Chem. Eur. J.,* 2013, **19**, 2889.

12 Q. Wang, M. Safdar, Z. Wang and J. He, *Adv. Mater.,* 2013, **25**, 3915.

13 G. Zhang, H. Fang, H. Yang, L. A. Jauregui, Y. P. Chen and Y. Wu, *Nano Lett.,* 2012, **12**, 3627.

14 N. Kim, S. Kee, S. H. Lee, B. H. Lee, Y. H. Kahng, Y. -R. Jo, B. -J. Kim and K. Lee, *Adv. Mater.,* 2014, **26**, 2268.

15 Y. Xia, K. Sun and J. Ouyang, *Adv. Mater.,* 2012, **24**, 2436.

16 K. C. See, J. P. Feser, C, E, Chen, A. Majumdar, J. J. Urban and R. A. Segalman, *Nano Lett.,* 2010, **10**, 4664.

17 J. Fu, S. Song, X. Zhang, F. Cao, L. Zhou, X. Li and H. Zhang, *CrystEngComm.,* 2012, **14**, 2159.

18 H. Ju, M. Kim and J. Kim, *Chem. Eng. J.,* 2015, **275**, 102.

19 E. J. Menke, M. A. Brown, Q. Li, J. C. Hemminger and R. M. Penner, *Langmuir,* 2006, **22**, 10564.

20 B. Poudel, Q. Hao, Y. Ma, Y. Lan, A. Minnich, B. Yu, X. Yan, D. Wang, A. Muto and D. Vashaee, *Science,* 2008, **320**, 634.

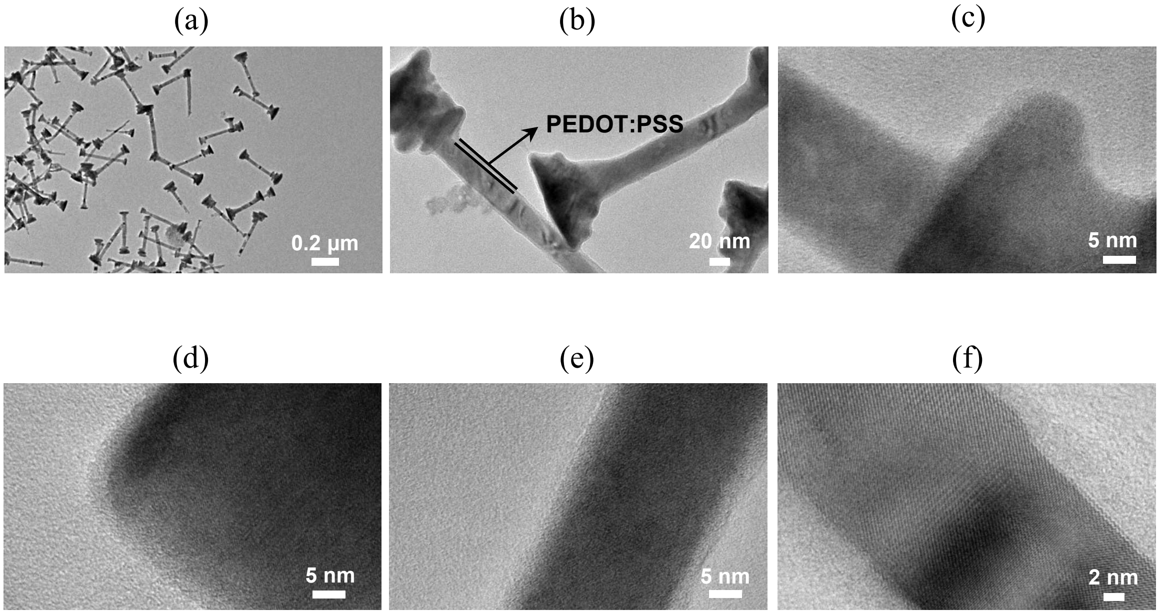

Figure 1. TEM images of Te–Bi_2Te_3/PEDOT:PSS hybrids: (a, b) nano-barbell structures of Te–Bi_2Te_3 nanowire heterostructures coated with PEDOT:PSS, (c) the junction between the nanobar (Te) and plate (Bi_2Te_3) part, (d) high magnification of the plate part, (e) high magnification of the nanobar part, and (f) crystalline phase in the hybrid.

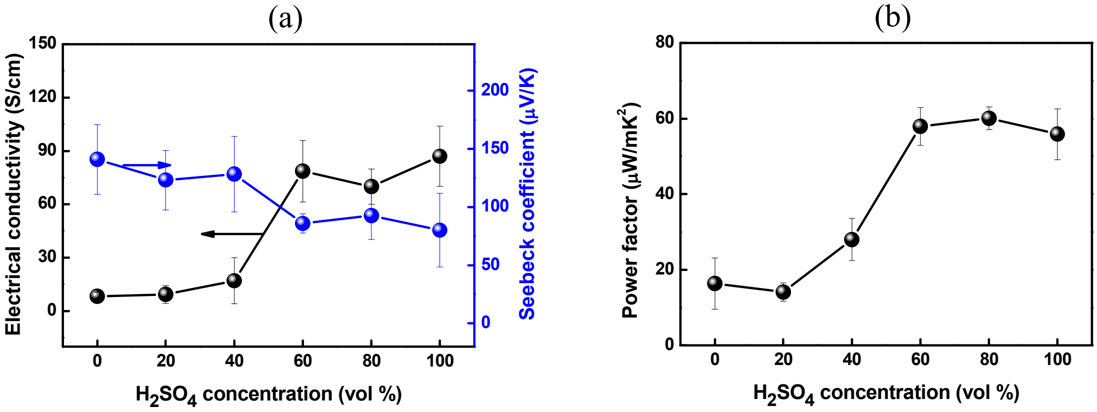

Figure 2. Thermoelectric properties of Te–Bi_2Te_3-PEDOT:PSS hybrid films treated with various concentrations of H_2SO_4: (a) electrical conductivity (black circle) and Seebeck coefficient (blue circle) and (b) power factor.

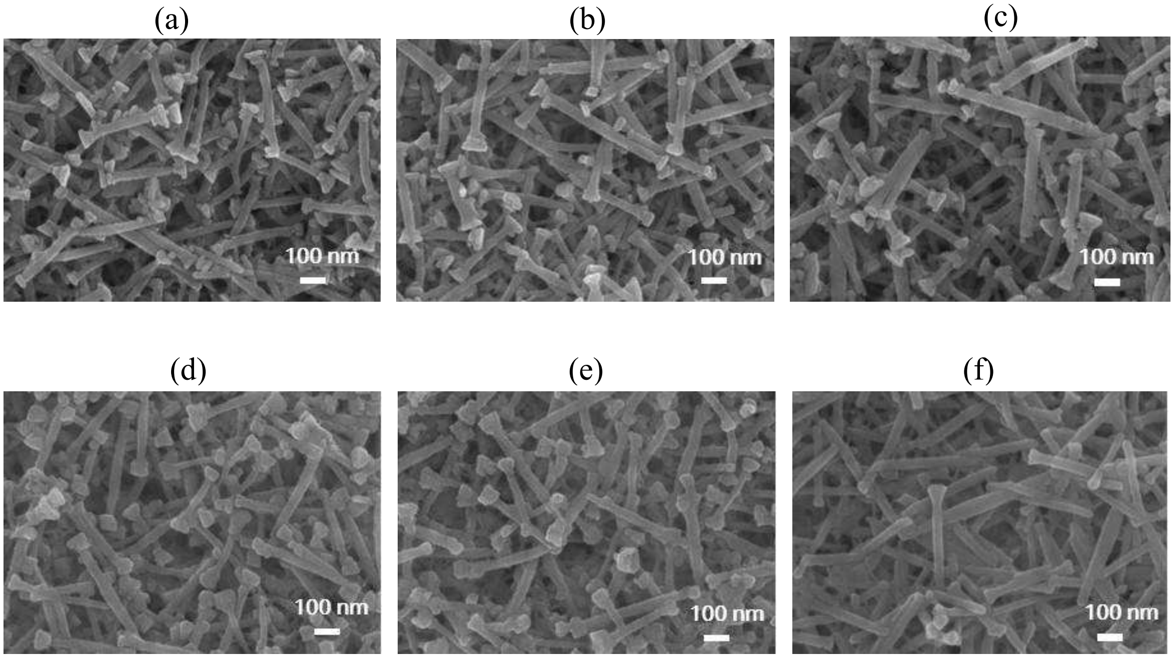

Fig. 3 Surface SEM images of Te–Bi_2Te_3/PEDOT:PSS hybrid films treated with various concentrations of H_2SO_4: (a) 0, (b) 20, (c) 40, (d) 60, (e) 80, and (f) 100 vol%, respectively.

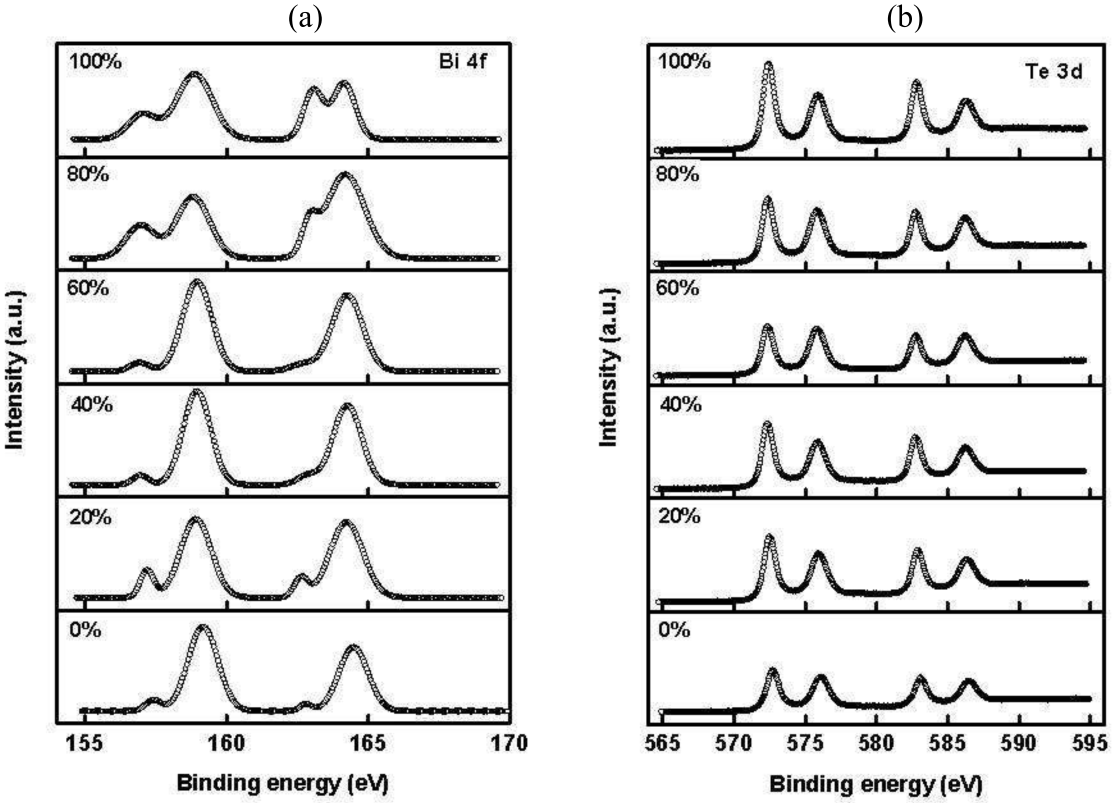

Fig. 4 XPS spectra of Te–Bi_2Te_3/PEDOT:PSS hybrid films treated with various concentrations of H_2SO_4: (a) Bi 4f and (b) Te 3d.

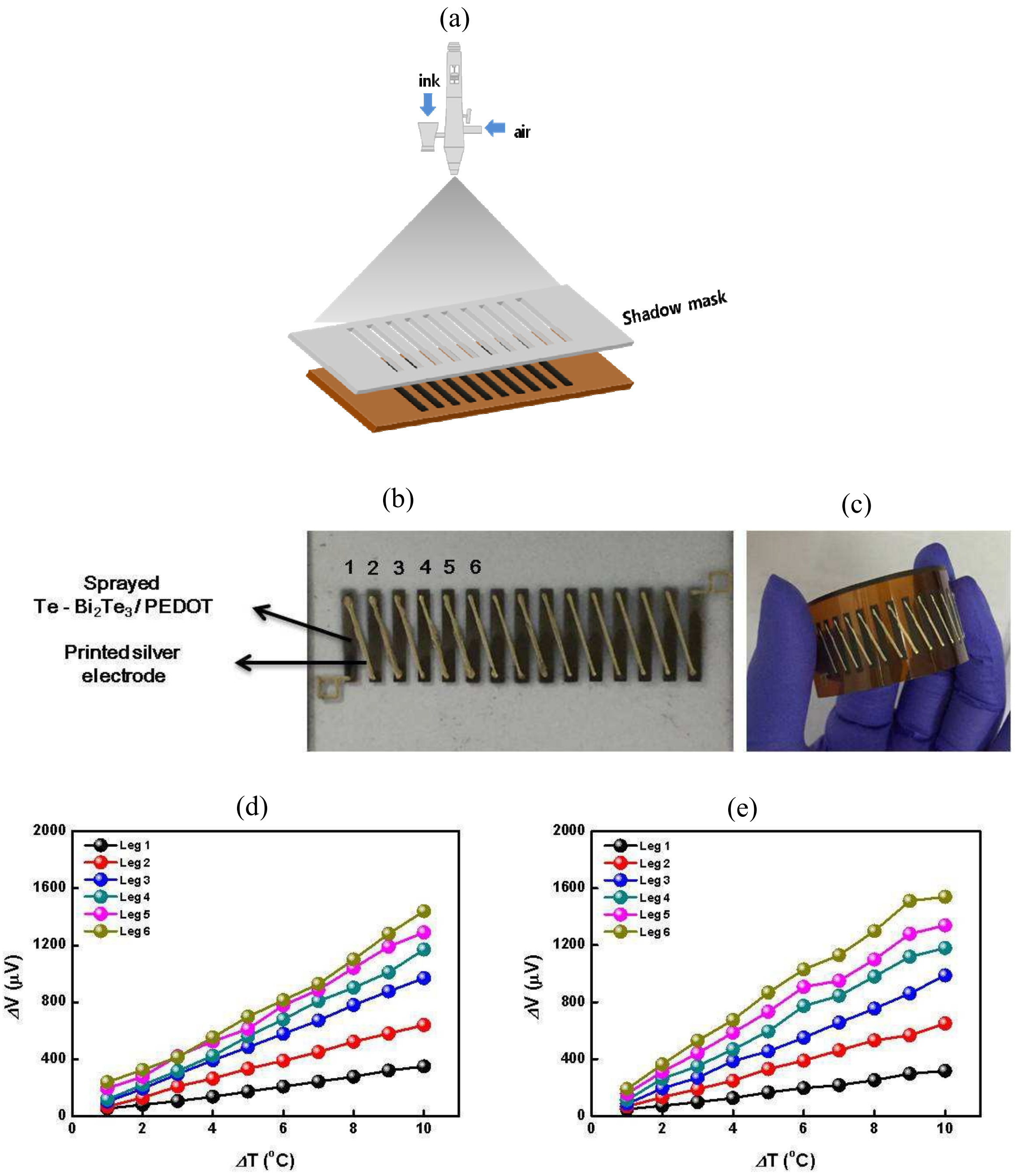

Fig. 5 (a) Schematic drawing of the spray-printing process, (b) image of the planar thermoelectric generator consisting of 15 legs arranged on the glass substrate, (c) image of the flexible thermoelectric generator, and (d, e) open circuit thermoelectric voltage (V_{oc}) *vs.* temperature difference (*Δ*T) according to the number of TE legs of rigid and flexible TE generators.